Role of Nonthermal Velocity Fluctuations on Anomalous Impurity Heating in the TJ-I Tokamak

B. Zurro, J. Vega, F. Castejón, and C. Burgos
Asociación EURATOM/CIEMAT para Fusión, E-28040 Madrid, Spain
(Received 23 June 1992)

Measured impurity temperature profiles from linewidths in the TJ-I tokamak are shown to be higher than proton temperature profiles. The difference between both apparent temperatures, which is attributed to the presence of anisotropic nonthermal velocities, tends to decrease as the density increases. Whereas electrostatic drifts due to $\tilde{\mathbf{E}}\times\mathbf{B}$ might be responsible for the poloidal turbulence velocities, radial velocities might be dominated by magnetic turbulence. These conclusions are supported by criteria based on the radial dependence and typical strengths of electric and magnetic fluctuations.

PACS numbers: 52.25.Vy, 52.25.Gj, 52.35.Ra, 52.70.Kz

Spatially resolved measurements of Doppler temperatures of protons and impurities in the TJ-I tokamak do not fit the generally accepted framework used for linewidth data interpretation in tokamaks [1]. Within this framework, it is expected that due to the density and toroidal field ranges of these experiments the linewidth is dominated by thermal Doppler broadening, i.e., Stark and Zeeman effects as well as the influence of plasma turbulence are ignored. Strong collisional coupling assures thermalization of different species.

Apparent impurity temperatures in TJ-I are often substantially higher than proton temperatures, even though the temperatures are expected to be the same from collisional coupling [2]. Anomalous impurity temperatures have also been reported in several magnetic confinement devices ([3,4] and other references therein). This anomaly might be due to non-Coulombic processes or to mass motions. The distinction between anomalous ion heating due to non-Coulombic processes and the additional line broadening caused by gross mass motions is difficult to make when using a single ion or when spatially resolved measurements are not available. However, since nonthermal velocities may scale more distinctly with density and spatial position than thermal velocities, scaling of apparent temperatures with these parameters can help in its interpretation. It seems reasonable to attribute the anomaly to non-Coulombic processes when the time for temperature equilibrium among different species is short enough and all the species together exhibit a higher temperature than that predicted from classical electron-ion equilibration. The effect can be triggered, for instance, in current-carrying plasmas at high values of the electron-streaming parameter [5]. However, if the impurities show a higher apparent temperature than protons, and this effect is not due to a long equilibration time between species, the apparent temperatures may reflect nonthermal processes.

If the nonthermal velocities due to plasma fluctuations are assumed to produce a Gaussian contribution to the linewidth, the actual measured linewidth, after deconvolving it by the instrumental function, will be given by $\Delta\lambda^2=\Delta\lambda_T^2+\Delta\lambda_{NT}^2$, where T and NT stand for thermal and nonthermal, respectively. If the nonthermal width does not depend on the charge and mass of the particle, its manifestation for protons and impurity ions with long ionization times will be different and can be unambiguously identified. This effect, which has been used in astrophysics (see Ref. [6]) to study the plasma turbulence in astronomical objects, has not been identified prior to this Letter in laboratory plasmas. We claim in this Letter, based on TJ-I tokamak data, that low-level fluctuating fields can induce observable effects over some linewidths due to this mechanism. Experimental profiles of proton and impurity temperatures, in combination with a data analysis code described in [7], have been used to deduce in this tokamak the anisotropic spatial structure of nonthermal velocity fluctuations. A discussion on the electrostatic or magnetic origin of these anisotropic velocities is addressed.

This experiment was carried out in the TJ-I tokamak, $R_0=30$ cm and $a=10$ cm. It was operated for this experiment with a plasma current of around 40 kA, a toroidal field of 1 T, and line-averaged electron densities between 0.5×10^{13} and 3×10^{13} cm^{-3}. The device and diagnostics are described in more detail in Ref. [2]. Discharges with Z_{eff} close to 2 at moderate densities are achieved. Discharges free of observable Mirnov activity were selected, but sawteeth activity of small relative amplitude (5%) was present in some of them. Spatially resolved measurements of impurity and proton temperatures have been deduced from Doppler line broadening of hydrogen (line wings) and impurity lines (i.e., C V, 2271 Å), with corrections made for the instrumental function. Measurements are performed with a 1-m monochromator having a multichannel intensified detector attached to its focal plane, and the spectrometer system is operated in first-third diffraction orders with 10^5–10^6 resolution. Spatial resolution of 1.5 cm is achieved by varying the optical line of sight on a shot to shot basis, which allows coverage of the entire plasma cross section.

The influence of plasma turbulence on spectral linewidths has been included following the method used in astrophysics [6]. If the spectral line shape is the result of the convolution of a thermal Gaussian distribution and a turbulent Gaussian one, the latter producing a gross mass motion, the full width at half maximum of the resulting

line is given by $\Delta\lambda = 1.665(\lambda/c)(2kT/m_i + \xi^2)^{1/2}$, where ξ is the dispersion of the Gaussian microturbulence velocity distribution, λ is the spectral line wavelength, c the light velocity, T the ion temperature, k the Boltzmann constant, and m_i the ion mass. The value of ξ is the most probable velocity and is $\sqrt{2}$ times larger than the root-mean-square (rms) value. If this turbulent velocity is assumed to be due to $\tilde{\mathbf{E}}\times\mathbf{B}$ drifts, their components in the radial, poloidal, and toroidal directions are given by

$$\tilde{v}_r = \frac{\tilde{E}_p}{B}, \quad \tilde{v}_p = \frac{\tilde{E}_r}{B}, \quad \tilde{v}_t = \frac{\tilde{E}_r B_p}{B^2} \ll \tilde{v}_p .$$

Radial magnetic fluctuations, possibly increasing towards the center in tokamaks, might not have a negligible influence on the radial fluctuating velocities of the ions, and may contribute significantly when the plasma is observed along central chords. Its effect can be estimated, for rms values, by the expression

$$\tilde{v}_r \cong (v_\parallel \tilde{B}_r/B_T)(2N\tau_p)^{1/2},$$

where $v_\parallel$ is the ion parallel velocity; the second factor is the relative radial magnetic fluctuation, with N the number of gyro-orbits per second performed by the ion, in each of which two small random perturbations occur, and τ_p the ion effective confinement time. Radial fluctuating velocities are, according to this picture, the result of a cumulative process of a set of small random perturbations. An analogous argument has been used to simulate the effect of magnetic fluctuations on ion diffusivity [8]. Therefore, when observation is performed perpendicular to the torodial field and along chords lying in a plane perpendicular to the equatorial plane, $\tilde{v}_p$ produces the dominant contribution for peripheral chords, because its projection along the line of sight is maximum. Therefore, $\tilde{v}_p$ can produce impurity temperature profiles that do not decrease to low values at the edge as long as nonthermal velocities are not negligible compared with thermal ones. On the other hand, $\tilde{v}_r$ is relevant for enhancing central linewidths when the poloidal component contribution is zero.

The data analysis method [7] divides the plasma in fifty circular concentric shells and within each of them plasma parameters are constant. It assumes a Gaussian impurity emissivity profile, whose width and maximum position are varied up to the point when the chord-integrated emission profile fits the experimental one. Similarly, the code starts from a local temperature profile slightly lower than that deduced from the H_β wings to account for the smaller effect of the nonthermal velocities on protons. The chord-averaged impurity temperature profile is simulated by averaging a set of Gaussians, whose widths are a function of the local temperature and nonthermal velocities, weighted by the emissivity and length of the ray in each particular shell. The coefficients defining the strength and radial dependence of the assumed anisotropic turbulence velocities are varied up to the point when the calculated apparent chord temperature profile matches the experimental one. Other effects such as plasma rotation and Zeeman effect, also included in the code, are less important for this analysis.

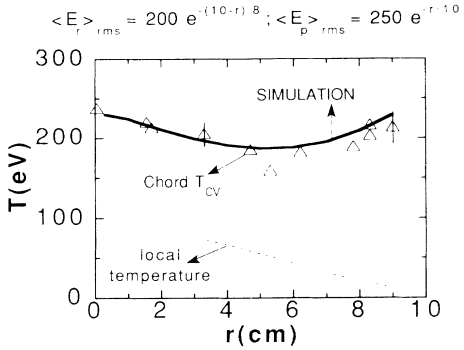

FIG. 1. Plot of experimental chord-averaged impurity and local proton temperature profiles in a low density TJ-I discharge, $\bar{n}_e = 1\times10^{13}$ cm^{-3}. The simulated curve was obtained with anisotropic nonthermal velocity fluctuations included. Equivalent fluctuating electric field values and radial dependence are given at the top of the figure.

The method outlined above has been used to account for the different apparent temperature profiles of protons and impurities observed in the TJ-I tokamak. In Figs. 1, 2, and 3, we show proton and impurity temperature profiles for C V at three different electron densities: (1, 2, and 3)$\times10^{13}$ cm^{-3}. The impurity temperature (chord averaged) is higher than the local proton one. This effect is noticeable in the lowest density case (Fig. 1) for any plasma chord. Even for the highest density case (Fig. 3), the effect can be clearly seen at the plasma periphery. Whereas the proton temperature increases with density, the impurity temperature diminishes with density. The

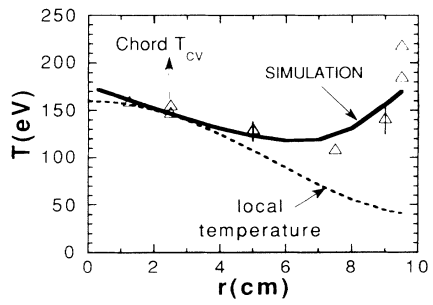

FIG. 2. Plot of experimental chord-averaged impurity and local proton temperature profiles for an intermediate density, $\bar{n}_e = 2\times10^{13}$ cm^{-3}. Notice that the discrepancy between both temperatures for central chords has almost disappeared, but since the impurity temperature is chord averaged and the proton one is a local value, some enhancement is needed for explaining this behavior. High impurity temperatures at the plasma periphery are clearly observable in this plot. The simulated curve obtained, as in Fig. 1, is also given.

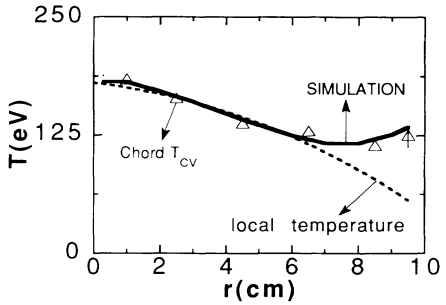

FIG. 3. Similar plot to those of Figs. 1 and 2 for a high density case ($\bar{n}_e = 3\times10^{13}$ cm^{-3}). Notice that even at this high density, the difference between chord-averaged impurity temperature and the local proton temperature is clearly seen at the plasma periphery. The upward wings in the impurity temperature profiles of previous cases are reduced at this density. Simulated chord-integrated temperature profile appears also superimposed in this figure.

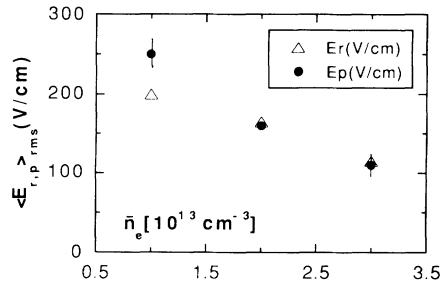

FIG. 4. Plot of root-mean-square fluctuating velocities or equivalent electric field values (radial and poloidal) vs density. The turbulence strength was described by an exponential function and it was assumed to peak at the plasma edge for the radial component and at the center for the poloidal one, in order that the model describe the experimental behavior of the impurity temperature profile.

local temperature profile is obtained from the H_β line wings and the charge-exchange neutral analyzer at the center [2], both methods giving results at the center in reasonably good agreement; for the rest of the profile only the optical method has been used. In both methods the fit to the neutral energy distribution is performed in the tail, for energies 5–10 times higher than proton temperature. In the density range covered in this experiment the central electron temperature varies between 400 eV (low density) and 250 eV (high density). The simulated profiles of Figs. 1–3 were obtained starting from the local temperature profile and applying the simulation code explained before, including a significant level of radial and poloidal fluctuating velocities in the expression for the linewidth given above. Those velocities are given in equivalent fluctuating electric fields, whose possible origin we will discuss. $\tilde{E}_r$(rms) or $\tilde{v}_p$ were described by an exponential function with its maximum at the plasma edge, and $\tilde{E}_p$(rms) or $\tilde{v}_r$(rms) were chosen with a maximum at the plasma center. Gaussian functions peaking at similar radii could also provide a reasonable fit. Peak values (V/cm, rms) and decay lengths (cm) of the Gaussian fluctuating fields for explaining this behavior are given in the plot for the low density case. These parameters were iteratively varied to obtain the best agreement between the simulated chord-averaged temperature profile and experiment, with a final uncertainty of between 10% and 15%.

In Figs. 4 and 5, the results of this type of profile analysis at three different electron densities are shown. We have chosen the plasma density since it is the most significant parameter to produce a clearly observable influence on this effect. In Fig. 4, the rms value of the equivalent Gaussian fluctuating electric field is plotted, versus the line-averaged electron density, for the poloidal and radial components. Similarly, Fig. 5 is a plot of the radial decay length, i.e., the fitted width of the radial distribution fluctuation amplitudes. As can be seen, the turbulence level characterized by these two parameters, needed to explain the impurity temperature behavior, decreases in both intensity and radial extension as density increases.

The rms value and radial dependence of the radial fluctuating electric field are consistent with Langmuir probe data in tokamaks [9], of around 150 V/cm in TEXTOR at 3×10^{13} cm^{-3}, versus 1220 V/cm in this work. In contrast, the inferred radial dependence of the equivalent poloidal fluctuating electric fields has a behavior opposite to that expected for electrostatic turbulence, which should diminish from the edge in. Its edge value at the highest density, 15 V/cm, is close to typical values of 20 V/cm measured in TJ-I and other tokamaks [9].

An alternative explanation, not considered to date, of the radial fluctuating velocities could be based on the existence of radial magnetic fluctuations. This hypothesis is supported by two observations. First, the dependence of

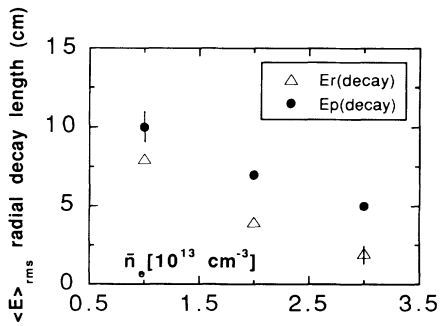

FIG. 5. Plot for radial decay length of the anisotropic Gaussian fluctuating velocities or equivalent electric fields vs line-averaged electron density. This parameter represents the decay constant of the exponential function assumed to describe the strength of the turbulence.

the deduced radial fluctuating velocities (rms) with radius, peaking at the center and decaying toward the edge, is as expected for the radial magnetic fluctuations [10, 11]. Second, magnetic fluctuations with typical values of $v_{\parallel}$ [$(3-6)\times 10^6$ cm/sec] and $\tilde{B}_r/B_T$ (10^{-4}–10^{-3}) would account for the central observed values of v_r. According to this interpretation the poloidal fluctuating velocities would be dominated by radial fluctuating electric fields and the radial fluctuating velocities by radial magnetic fluctuations. In fact, the time evolution of the anomalous impurity temperature of O V, higher than the proton one, measured in a reverse field pinch [12], correlates with the magnetic fluctuation level.

Since TJ-I plasma conditions are similar to those existing at the edge of large devices, this work has two important consequences for fusion relevant plasmas. First, the high edge ion temperature reported in JET [13] and other tokamaks, which is obtained mainly from the Doppler linewidth of impurity lines, might be due to a similar effect. Second, central heavy impurities in JET [14], when corrected by spatial averaging effects, exhibit higher temperature than light impurities which might be explained by a similar mechanism, as has been already pointed out [15].

This research was supported by the Ministry of Science and Education, DGCYT Project No. PB90-0410.

[1] R. Isler, Nucl. Fusion **24**, 1599 (1984).

[2] B. Zurro, C. Hidalgo, B. García-Castañer, and C. Pardo, Plasma Phys. Controlled Fusion **32**, 565 (1990).

[3] A. Fujisawa, H. Ji, K. Yamagishi, S. Shinohara, H. Toyama, and K. Miyamoto, Nucl. Fusion **31**, 1443 (1991).

[4] J. M. McChesney, P. M. Bellan, and R. A. Stern, Phys. Fluids B **3**, 3363 (1991).

[5] A. A. M. Oomens, L. Th. M. Ornstein, R. R. Parker, F. C. Schuller, and R. J. Taylor, Phys. Rev. Lett. **36**, 255 (1976).

[6] D. F. Gray, *Lectures on Spectral-Line Analysis: F, G, and K Stars* (Aylmer Express, Aylmer, Ontario, 1988).

[7] B. Zurro and C. Burgos, Rev. Sci. Instrum. (to be published).

[8] J. T. Mendonca and M. Brusati, in Proceedings of the Seventeenth European Conference on Controlled Fusion Plasma Heating (unpublished).

[9] D. Bora, R. S. Ivanov, G. Van Oost, and U. Samm, Nucl. Fusion **31**, 2383 (1991).

[10] D. E. Graessle, S. C. Prager, and R. N. Dexter, Phys. Rev. Lett. **62**, 535 (1989).

[11] S. J. Zweben and R. J. Taylor, Nucl. Fusion **21**, 193 (1981).

[12] T. Fujita, K. Saito, J. Matsui, Y. Kamada, H. Morimoto, Z. Yoshida, and N. Inoue, Nucl. Fusion **31**, 3 (1991).

[13] H. Weisen, H. Bergsaker, D. J. Campbell, S. K. Erents, L. C. J. M. de Kock, G. M. McCraken, M. F. Stamp, D. D. R. Summers, P. R. Thomas, M. Von Hellermann, and J. Zhu, Nucl. Fusion **31**, 2247 (1991).

[14] M. Danielsson, M. G. von Hellermann, E. Kallne, W. Mandl, H. W. Morsi, H. P. Summers, and K. D. Zastrow, Rev. Sci. Instrum. **63**, 2241 (1992).

[15] G. Fussman, Report No. JET-R12, 1987 (unpublished).